Rotational stiffness of radial joints in segmental linings

In this article, Benoit Jones looks at the rotational stiffness of segmental lining joints with packers

IN THE FEBRUARY-MARCH 2015 ISSUE of Tunnelling Journal (Jones, 2015) we looked at radial joints in segmental linings (sometimes referred to as 'longitudinal joints') and the shortcomings of analytical solutions that either assume completely free rotation of joints or a monolithic lining. In this article we will delve deeper into the rotational stiffness of joints with packers in precast concrete segmental linings.

Introduction

Analytical solutions, such as the Curtis-Muir Wood method (Muir Wood, 1975; Curtis, 1974), have to assume a single value of lining stiffness that takes account of both the segment stiffness and the effect of joints. The two limiting situations are either that the radial joints are pin joints, providing no rotational stiffness, or that the lining is monolithic (i.e. as though there were no joints at all). De Waal (2000) showed, and perhaps it is intuitively obvious, that the true situation will always be somewhere between these two limiting situations. Fei et al. (2014) also proved this fact using scale models.

Lee & Ge (2001) proposed a method for back-calculating the effective bending rigidity of a tunnel lining based on its deformation, and this kind of approach could be used along with an analytical solution. However, since the effect of the joints is 'smeared' or averaged, the analytical solution will only predict average bending moments in the lining.

When using bedded beam models or finite element models of segmental linings, it is possible to model the joints explicitly using a rotational stiffness. However, the value of rotational stiffness is difficult to determine experimentally and detailed numerical modelling is often considered the only option. In this article we will explore some simple methods for estimating the rotational stiffness.

Conceptual model

What we want to estimate is a value for rotational stiffness. This is the bending moment per unit length (in the tunnel longitudinal direction) required to cause a unit rotation angle along a radial joint. According to full-scale tests by Teachavorasinskun & Chub-uppakarn (2010), typical values are 1000 – 3000 kNm/rad.

A transverse section of a radial joint experiencing rotation is shown in Figure 1. As the joint rotates, the contact stress distribution moves and the resultant hoop force in the lining moves away from the centreline. This eccentricity of hoop force generates a bending moment.

Figure 1 shows a contact stress distribution that one might expect from a linear elastic packer, and this is sometimes assumed in calculations because it is easy to solve. Nowadays, packers are most often made from bituminous or plastic (polyethylene or polyurethane based) materials. MDF or plywood is becoming less popular due to durability concerns (Cavalaro & Aguado, 2012). None of these materials behave in a linear elastic manner so to get a reasonable estimate of rotational stiffness we need to develop that assumption into something a bit more sophisticated.

Linear elastic packer model

We are going to start with a simple linear elastic packer model to explain the steps. Figure 2 shows the geometry and symbols we are going to use.

Figure 1: Section through a radial joint experiencing rotation

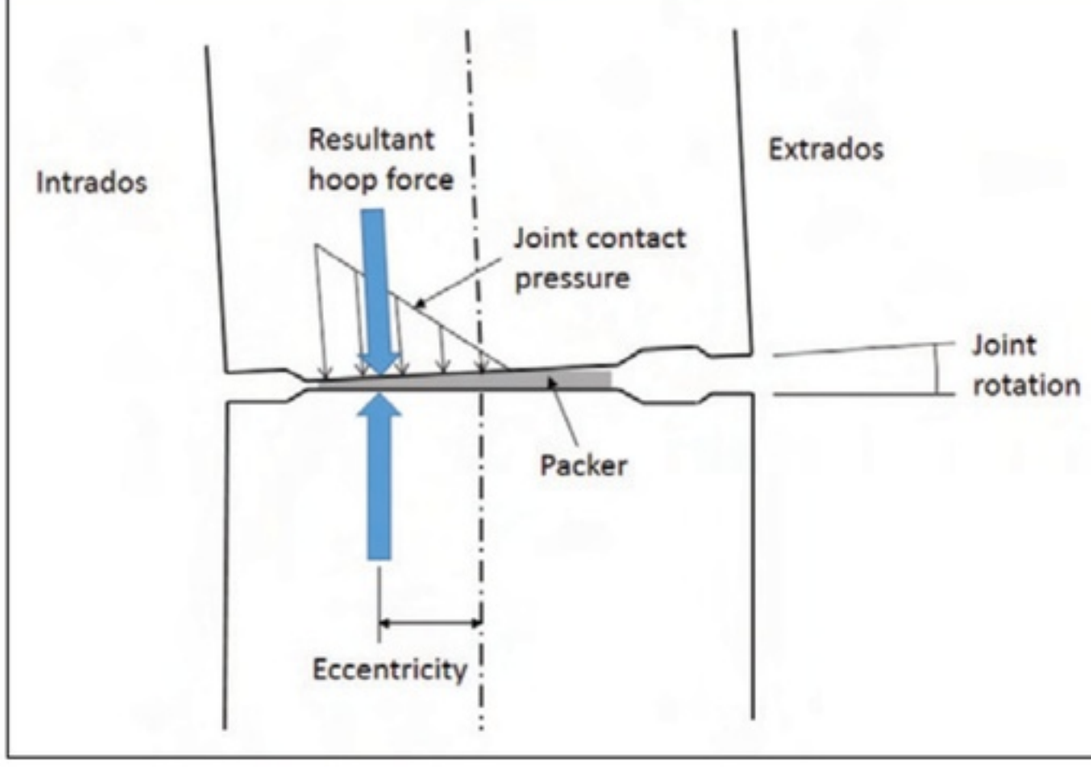

Figure 2: Calculation of contact stress distribution - linear elastic packer

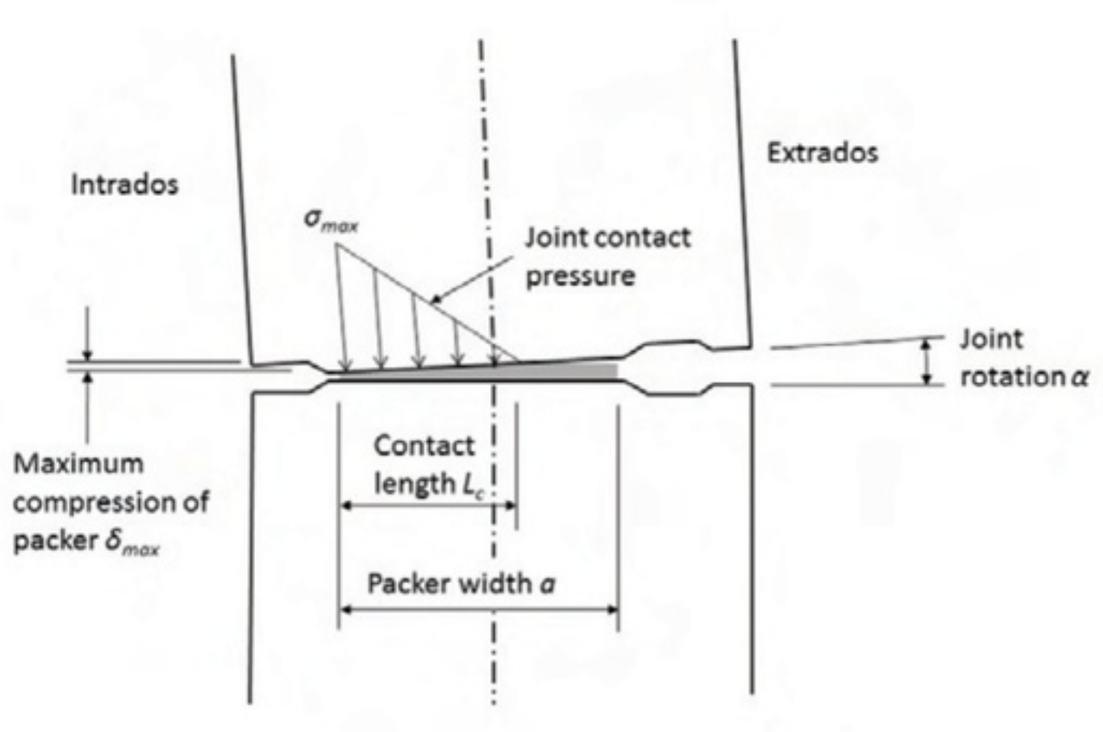

For simplicity it is assumed that the packer is symmetrically positioned on the centreline of the joint. The packer is linear elastic, with Young's modulus E_p, so it follows from Hooke's Law that the maximum compression displacement of the packer δ_{max} is given by:

$$\delta_{max} = \frac{\sigma_{max} t_p}{E_p} \quad [1]$$

Where σ_{max} is the maximum stress as shown in Figure 2, t_p is the thickness of the packer and E_p is the Young's modulus of the packer.

Also, the area of the triangle must equal the hoop force N in the segment for there to be equilibrium:

$$N L_s = \frac{\sigma_{max} L_c L_p}{2} \quad [2]$$

Where L_s is the segment length in the tunnel longitudinal direction, L_c is the contact length as shown in Figure 2 and L_p is the length of the packer in the tunnel longitudinal direction (as it won't be covering the full length of the segment).

Rearranging equation [1] for σ_{max} and substituting it into equation [2] gives:

$$N = \frac{\delta_{max} E_p L_c L_p}{2 t_p L_s} \quad [3]$$

Now we have 2 unknowns, δ_{max} and L_c, but they are related geometrically by the following equation [4]:

$$L_c = \frac{\delta_{max}}{\alpha} \quad [4]$$

Substituting equation [4] into equation [3] gives:

$$N = \frac{\delta_{max}^2 E_p L_p}{2 t_p \alpha L_s} \quad [5]$$

Rearranging for δ_{max} gives us:

$$\delta_{max} = \sqrt{\frac{2 t_p \alpha L_s N}{E_p L_p}} \quad [6]$$

Using this equation, we can find the value of δ_{max} that gives us equilibrium for a given value of hoop force N, packer properties E_p, L_p and t_p, and joint rotation α. We can then use this value of δ_{max} in equation [4] to find L_c. Once L_c is known, the position of the resultant hoop force can be found, in this case for a triangular distribution it will be $L_c/3$ from the position of σ_{max}.

If the calculated contact length L_c is greater than the packer width a, then it means that the contact pressure distribution is trapezoidal rather than triangular. This means the assumptions in equations [2] to [6] are invalid and we have to start again and these equations are shown below as equations [2a] to [6a].

The hoop force per segment is now in equilibrium with a trapezoidal pressure distribution varying from σ_{max} to σ_{min} over the full width of the packer a:

$$N L_s = \left(\frac{\sigma_{max} + \sigma_{min}}{2}\right) L_p a \quad [2a]$$

Now δ_{min} has a similar relationship to σ_{min} as δ_{max} has to σ_{max} in equation [1], so we end up with:

$$N L_s = \frac{E_p L_p a}{2 t_p} (2\delta_{max} - a\alpha) \quad [3a]$$

Solving for δ_{max} gives us:

$$\delta_{max} = \frac{N L_s t_p}{E_p L_p a} + \frac{\alpha a}{2} \quad [6a]$$

Because we know δ_{max} and the rotation angle α, δ_{min} can be calculated:

$$\delta_{min} = \delta_{max} - a\alpha \quad [6B]$$

Example calculation

Packer properties: width a = 150 mm, thickness t_p = 3 mm, packer length in tunnel longitudinal direction L_p = 900 mm and Young's modulus E_p = 40 MPa.

Segment properties: internal diameter ID = 6000 mm, segment thickness t_s = 250 mm, length in tunnel longitudinal direction L_s = 1000 mm.

Loading condition: hoop thrust N = 500, 1000, 1500, 2000, 2500 kN/m.

Joint rotations from α = 0° to 1° will be calculated in a spreadsheet for hoop thrusts N = 500, 1000, 1500, 2000 and 2500 kN/m.

An example of the spreadsheet calculation for α = 0.5° (= 0.008727 rad) and N = 1500 kN/m (= 1500 N/mm) is presented below.

Using equation [6]:

$$\delta_{max} = \sqrt{\frac{2 t_p \alpha L_s N}{E_p L_p}} = \sqrt{\frac{2\times3\times0.008727\times1000\times1500}{40\times900}} = 1.477 \text{ mm}$$

Then using equation [4]:

$$L_c = \frac{\delta_{max}}{\alpha} = \frac{1.477}{0.008727} = 169.257 \text{ mm}$$

Now $Lc > a$, so the contact stress distribution must be trapezoidal. Starting again using equation [6a] and [6b] instead:

$$\delta_{max} = \frac{N L_s t_p}{E_p L_p a} + \frac{\alpha a}{2} = \frac{1500\times1000\times3}{40\times900\times150} + \frac{0.008727\times150}{2} = 1.488 \text{ mm}$$

$$\delta_{min} = \delta_{max} - a\alpha = 1.488 - 150\times0.008727 = 0.179 \text{ mm}$$

Using equation [1] rearranged for σ_{max} and σ_{min}:

$$\sigma_{max} = \frac{\delta_{max} E_p}{t_p} = \frac{1.488\times40}{3} = 19.840 \text{ N/mm}^2$$

$$\sigma_{min} = \frac{\delta_{min} E_p}{t_p} = \frac{0.179\times40}{3} = 2.387 \text{ N/mm}^2$$

To check the answer is right we can check using the equilibrium equation [2a]:

$$N = \left(\frac{\sigma_{max} + \sigma_{min}}{2}\right) \frac{L_p a}{L_s} = \left(\frac{19.840 + 2.387}{2}\right) \times \frac{900\times150}{1000} = 1500 \text{ kN/m}$$

To find the eccentricity e of the resultant hoop force N from the joint centreline, we resolve moments about the centreline as follows:

$$NL_s e = \frac{(\sigma_{max} - \sigma_{min}) a L_p}{2} \times \left(\frac{a}{2} - \frac{a}{3}\right)$$

Therefore:

$$e = \frac{(19.480 - 2.387) \times 150 \times 900}{2 \times 1500 \times 1000} \times \left(\frac{150}{2} - \frac{150}{3}\right) = 19.635 \text{ mm}$$

So in this case the eccentricity e = 19.63 mm, and the bending moment M resisting rotation is $M = Ne$ = 29.45 kNm. We can then calculate that the (secant) rotational stiffness is M/α = 3375 kNm/rad.

Parametric study – linear elastic packer

Figure 3 shows the relationship between joint rotation and bending moment for a linear elastic packer as calculated in a spreadsheet using the equations in the preceding section. At higher values of joint rotation, the line changes from a straight line to a curve, and this corresponds exactly to the point at which the contact stress switches from a trapezoidal distribution to a triangular distribution. As one might expect, this transition from trapezoidal to triangular stress distribution occurs later at higher values of hoop force. The rotational stiffness, which is the gradient of the curves in Figure 3, therefore is only a constant while there is a trapezoidal stress distribution, but beyond the transition to a triangular distribution, it decreases (or becomes less stiff) as rotation increases.

Figure 3: Bending moment - joint rotation relationship for a linear elastic packer with Young's modulus 40MPa at different levels of hoop force

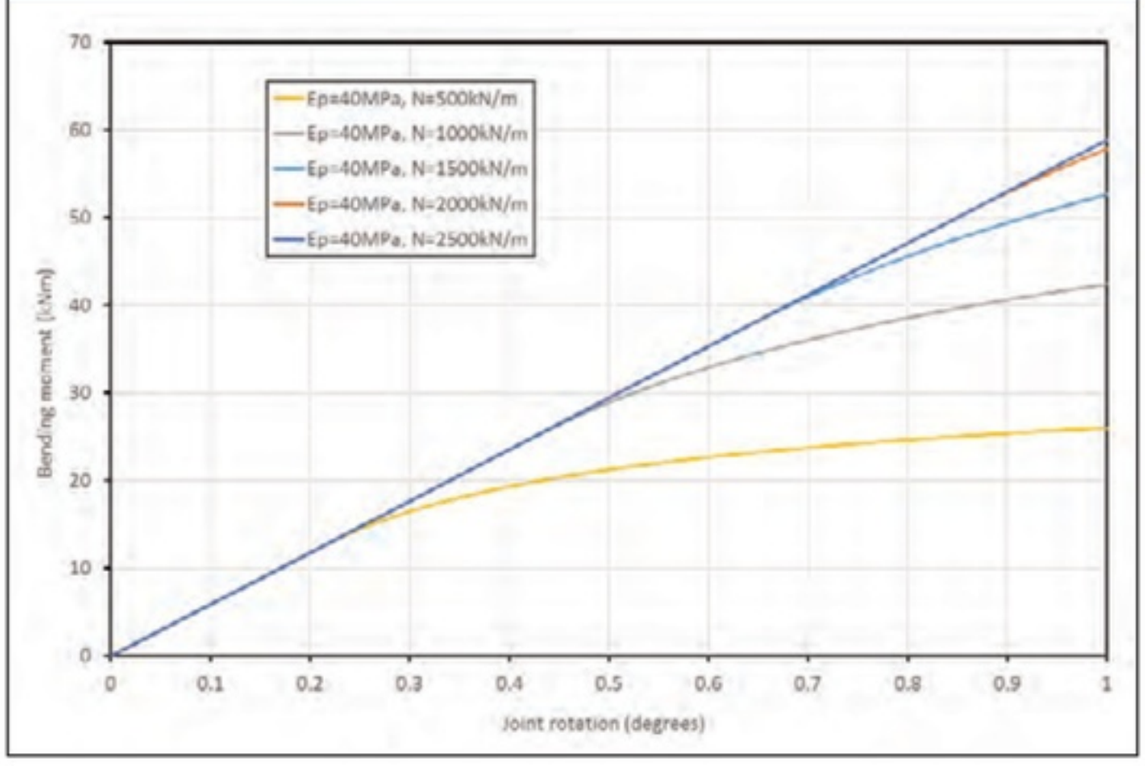

Figure 4: Contact stress distribution across a linear elastic packer as joint rotates under 1000 kN/m hoop force (note transition from trapezoidal to triangular stress distribution at approximately 0.43°)

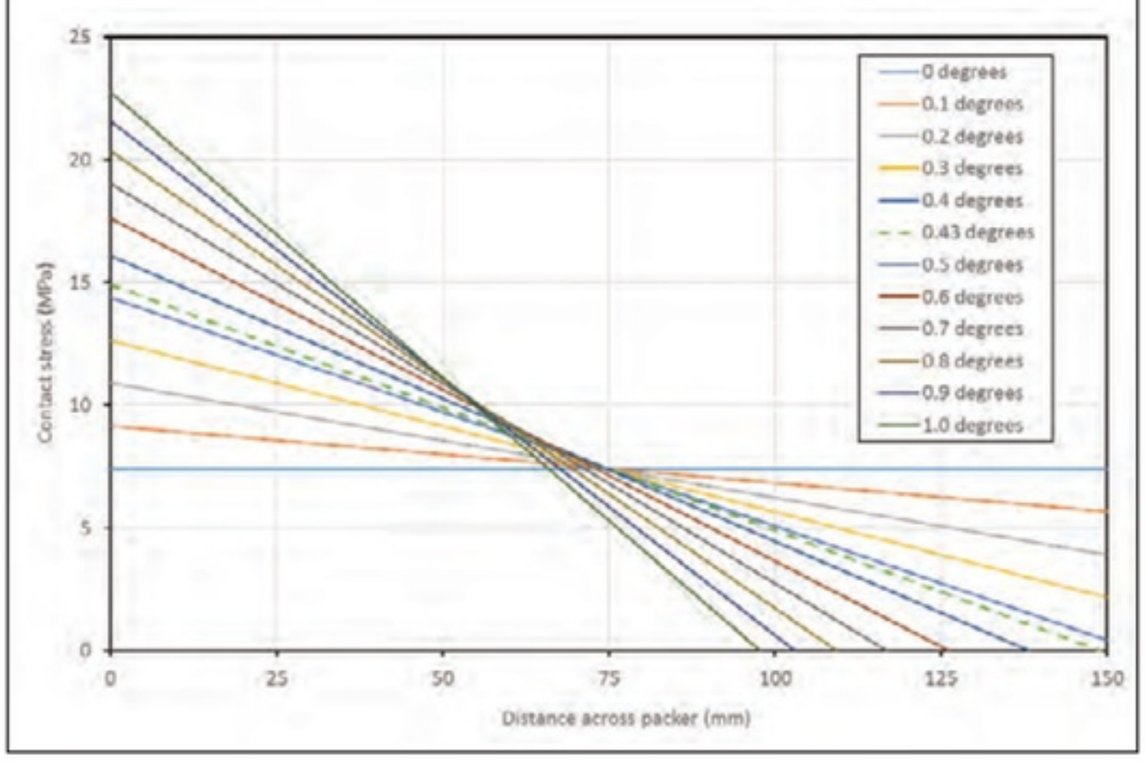

In order to illustrate the transition, the contact stress distributions for the hoop force of 1000 kN/m, as rotation is increased, are shown in Figure 4. At approximately 0.43 degrees, shown by the dashed line, the stress distribution switches from a trapezoidal shape to a triangular shape. Perhaps counterintuitively the eccentricity of the stress distribution (i.e. how far the centroid of the distribution is from the centreline) increases at an increasingly slower rate after the transition to a triangular distribution, and this results in the shape of the curves in Figure 3.

Nonlinear packer model

Cavalaro & Aguado (2012) performed tests on several types of packers used in projects in Spain. As an example, here we will use the stress-strain relationships Cavalaro & Aguado developed for a 1.92 mm thick bituminous packer and a 2.15 mm thick plastic packer, both used for the Barcelona Metro Line 9. The stress-strain relationship they propose has the form:

$$\sigma = A\left(1 - e^{-\varepsilon^n}\right)$$

Where A and n are curve-fitting parameters and ε is the strain.

This equation must have been a typographical error as it doesn't give anything like the correct curves. However, on investigation I found that this alternative matched the data perfectly, as long as you use the mm/m value of strain:

$$\sigma = A\left(e^{\varepsilon^n} - 1\right) \quad [7]$$

An important effect, particularly for bituminous packers, is that the first load cycle has a much softer response and on subsequent load cycles the material has a much stiffer behaviour. This is known as the 'Mullins effect' and is due to densification of the material. The stress-strain curves based on equation [7] and using the parameters in Table 1 are shown in Figure 5.

Figure 5: Stress-strain curves of plastic and bituminous packers plotted using equation [7]

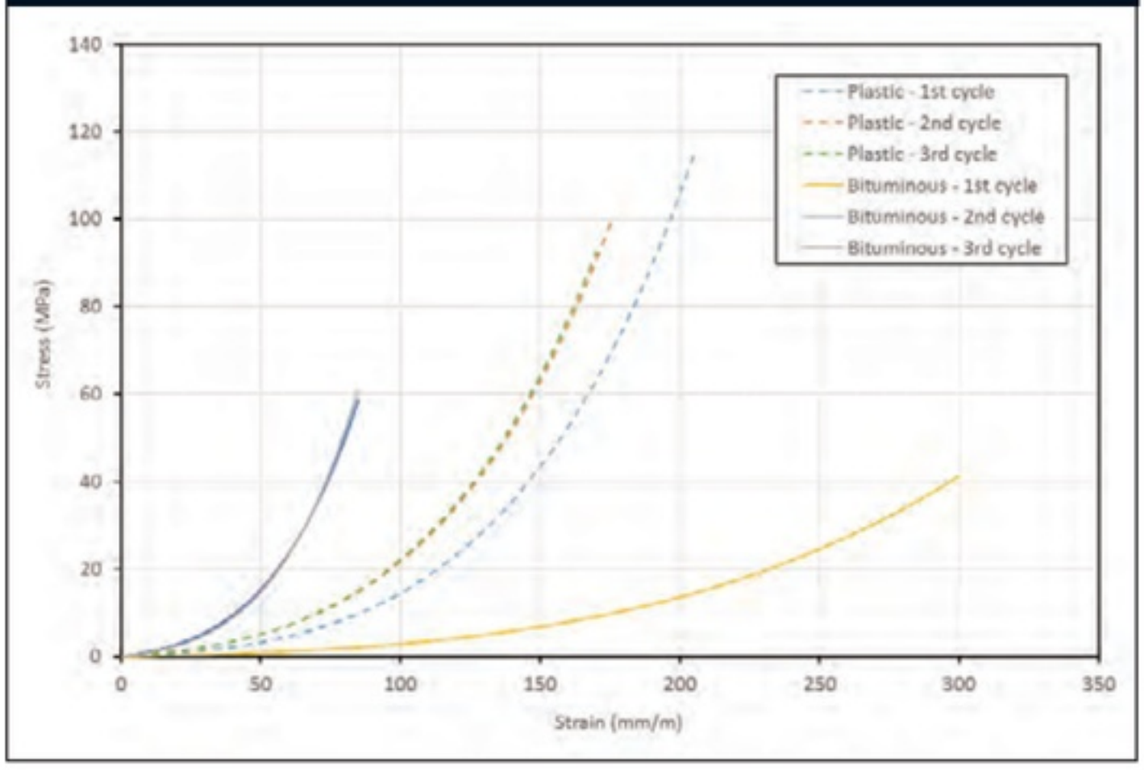

Table 1: Parameters from curve-fitting of tests on plastic and bituminous packers (from Cavalaro & Aguado, 2012)

	Code	Thickness t_p	A	n
Plastic 1st loading cycle	P1	2.15 mm	0.028	0.398
Plastic 2nd loading cycle	P2		0.047	0.394
Plastic 3rd loading cycle	P3		0.048	0.394
Bituminous 1st loading cycle	B1	1.92 mm	0.013	0.366
Bituminous 2nd loading cycle	B2		0.079	0.425
Bituminous 3rd loading cycle	B3		0.063	0.434

For brevity, we will try the parameters for only the 1st loading cycle of the plastic packer 'P1' as shown in Table 1.

The calculation is now a bit more complicated as the packer is nonlinear and we can't follow exactly the same procedure as for the linear elastic packer. Nevertheless, it can be done in a spreadsheet by dividing the width of the packer into slices and calculating the stress in each slice. The rotation angle is fixed and the maximum compression displacement δmax is varied using a 'goal seek' function until the integral of the stresses is in equilibrium with the hoop force.

The contact stress distributions as rotation is increased for the plastic packer with parameters P1 is shown in Figure 6. Compared to the linear elastic packer in Figure 4, the stress moves much more quickly to the side of the packer and attains much higher levels, but once there it changes less and less. This is because as the strain increases, the plastic packer becomes stiffer and stiffer, as is shown in Figure 5.

Figure 6: Contact stress distribution for plastic packer with parameters P1

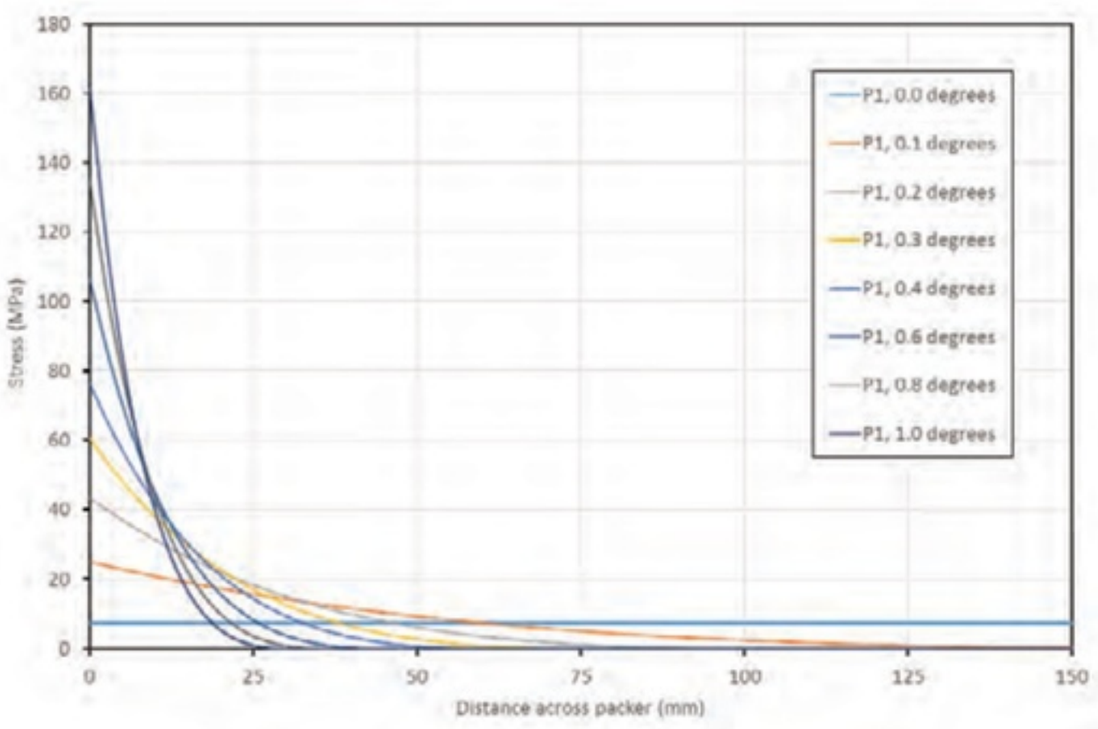

Figure 7: Contact stress distribution for 3mm plywood packer

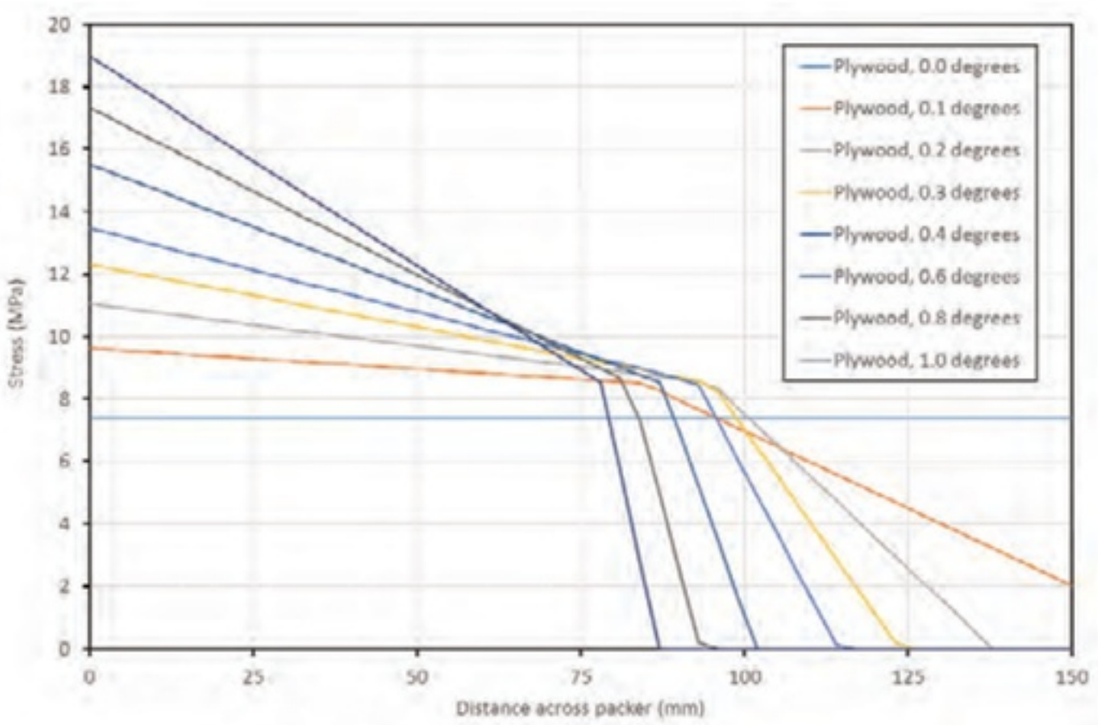

Another possibility is that a packer becomes less stiff as strain increases. This is the opposite of the plastic or bituminous materials we have just seen, but is typical behaviour of most engineering materials such as steel and concrete, and indeed other materials used as packers, such as plywood and MDF. Based on a compression test on a 3mm plywood packer that I found in some old design calculations, the following bilinear relationship could be assumed:

$E = 170$ MPa for $0 \leq \varepsilon \leq 0.05$

$E = 23$ MPa for $0.05 \leq \varepsilon \leq 0.5$

The contact stress distribution for a 3mm thick plywood packer is shown in Figure 7 for different values of joint rotation. The stress distribution is completely different in this case, being much more spread out and avoiding the very high values found at the edge of the plastic packer. Maximum compressive stresses are lower than for the linear elastic packer.

Effect on rotational stiffness

Figure 8 shows how the bending moment induced by eccentricity of contact stress develops as the joint rotates. The joint with a plastic packer develops much higher bending moments more quickly, as perhaps one might expect given the stress-strain relationship in Figure 5. The plywood packer also exhibits a nonlinear relationship but with a lower magnitude. The linear elastic packer (remember, this type of packer does not exist in the real world!) begins with a linear relationship between moment and rotation angle, but as the contact stress distribution transitions from a trapezoidal to a triangular shape, and the contact area begins to shrink, it also exhibits a nonlinear relationship.

Figure 8: Bending moment vs joint rotation for plastic, plywood and linear elastic packers, at a hoop force of 1000 kN/m

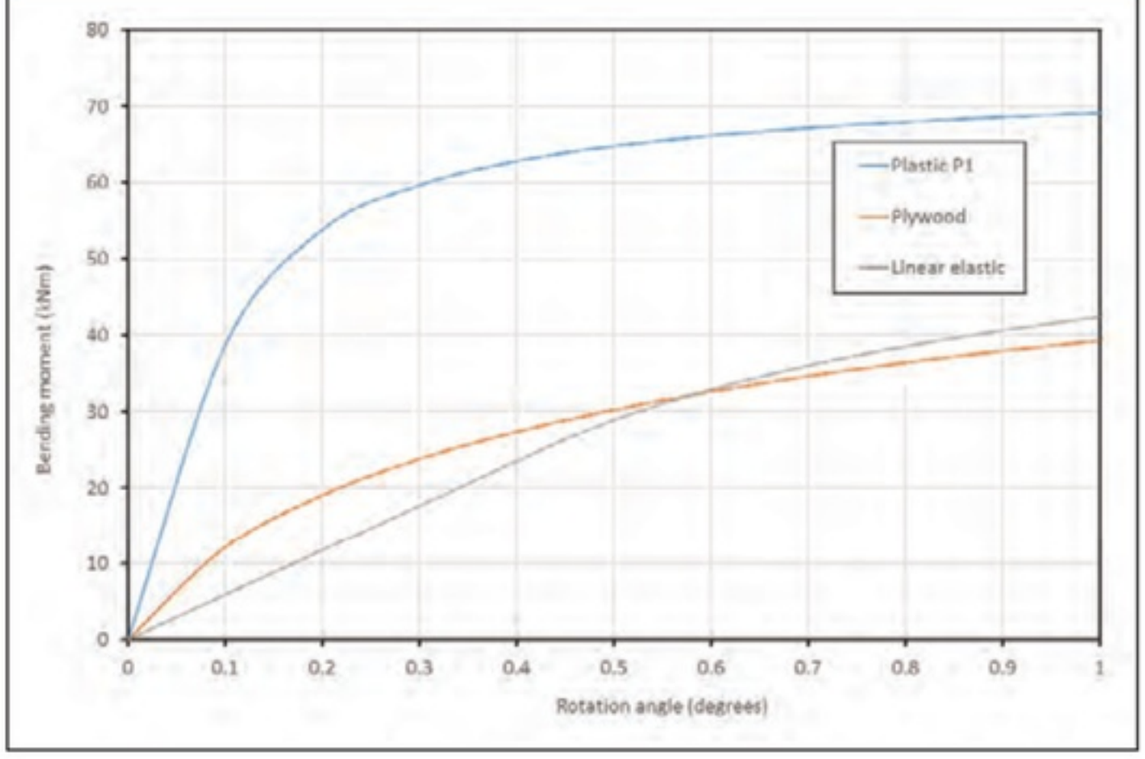

Since in all the cases the bending moment-joint rotation relationship is not linear, then there isn't a single value of rotational stiffness that can be used for a particular packer type. In Figure 9 the rotational stiffness is plotted against rotation angle for our example segment geometry, with the three different packers, and with a hoop force of 1000 kN/m. All packer types settle into a rotational stiffness of around 1000-3000 kNm/rad as found by Teachavorasinskun & Chub-uppakarn (2010), but at lower levels of joint rotation, rotational stiffness can be much higher.

Figure 9: Variation of rotational stiffness of joints with plastic, plywood and linear elastic packers with rotation angle, at a hoop force of 1000 kN/m

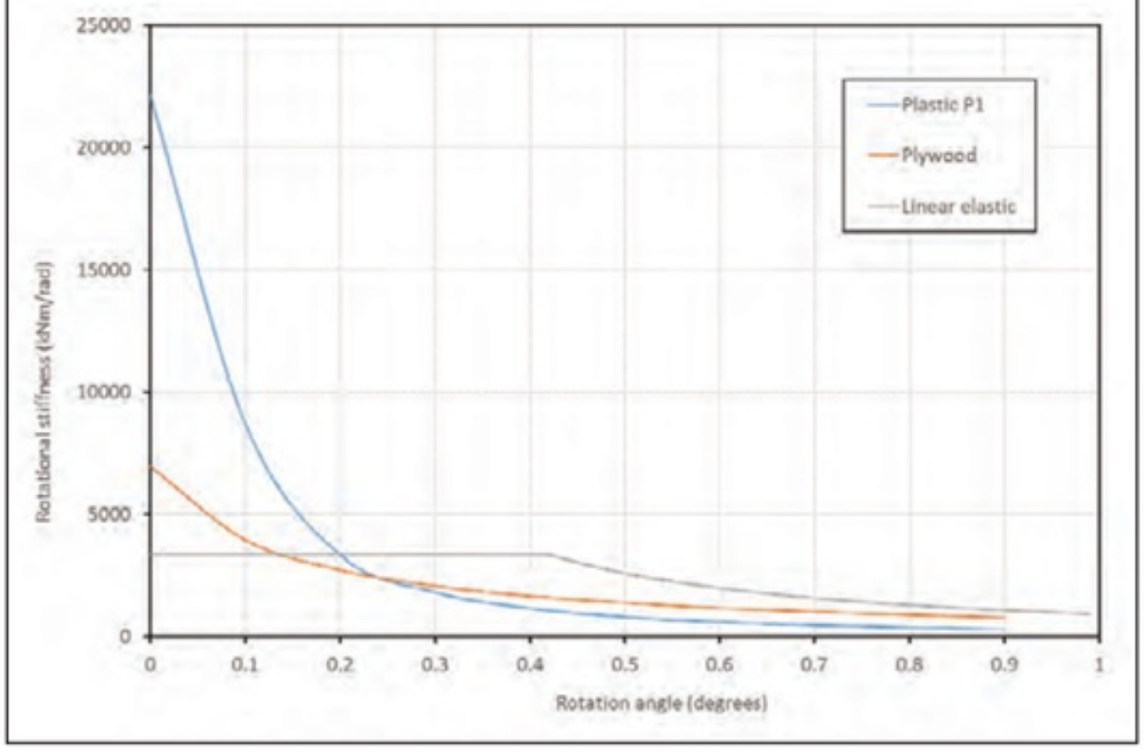

It is difficult to say what the effect of these very different behaviours is. For instance, a higher rotational stiffness will result in a higher overall ring stiffness, which will result in less deformation but higher bending moments. Also, the high stress concentrations at the edge of the packer that result from using a packer material that becomes stiffer at higher strain levels, such as plastic or bituminous packers, may have a knock-on effect on the design of the concrete segment itself in the vicinity of the joint.

It may be that these relationships between rotational stiffness and rotation angle need to be fed into a model of a tunnel, either a bedded-beam or a finite element model, in order to work out what the effect is. As always, all things are complex and inter-related, but that's what makes them interesting!

Conclusions

We talked about how the true behaviour of a segmental lining is somewhere between a pin-jointed ring of segments and a monolithic ring. These limiting cases are quite far apart, especially in terms of bending moments, which are crucial to design. Therefore, rotational stiffness of segmental lining joints is an important input to analysis of a tunnel if we want to improve confidence in our designs.

A simple calculation method was described for analysing the rotational stiffness of a packer.

We then looked at different packer types and found that their stress-strain behaviours can be very different to each other.

Finally, we have investigated the influence of the stress-strain behaviour of a packer on the contact stress distributions as a joint rotates, and that this has a big impact on the rotational stiffness. We also found that rotational stiffness varies with rotation angle.

REFERENCES

Cavalaro, S. H. P. & Aguado, A. (2012). Packer behavior under simple and coupled stresses. *Tunnelling and Underground Space Technology* 28, 159–173.

Curtis, D. J. (1974). Visco-elastic tunnel analysis. *Tunnels & Tunnelling, November,* 38-39.

De Waal (1999). R.G.A. (2000). *Steel Fibre Reinforced Tunnel Segments for the Application in Shield Driven Tunnel Linings*. PhD Thesis, Technische Universiteit Delft.

Fei, Y., Chang-fei, G., Hai-dong, S., Yan-peng, L., Yong-xu, X. & Zhuo, Z. (2014). Model test study on effective ratio of segment transverse bending rigidity of shield tunnel. *Tunnelling and Underground Space Technology* 41, 193–205.

Jones, B. D. (2015). Segmental lining joints. *Tunnelling Journal*, February/March issue, 38-40.

Lee, K.M. & Ge, X.W. (2001). The equivalence of a jointed shield-driven tunnel lining to a continuous ring structure. *Canadian Geotechnical Journal* 38, 461–483.

Muir Wood, A. M. (1975). The circular tunnel in elastic ground. *Géotechnique* 25, No.1, 115-117.

Teachavorasinskun, S. & Chub-uppakarn, T. (2010). Influence of segmental joints on tunnel lining. *Tunnelling and Underground Space Technology* 25, 490-494.